Journal of Solid State Chemistry 183 (2010) 1314–1325

Contents lists available at ScienceDirect

Journal of Solid State Chemistry

journal homepage: www.elsevier.com/locate/jssc

Magnetic properties of Fe_2P-type R_6CoTe_2 compounds (R=Gd–Er)

A.V. Morozkin [a,*], Yu Mozharivskyj [b], V. Svitlyk [b], R. Nirmala [c], O. Isnard [d,e], P. Manfrinetti [f,g], A. Provino [f,g], C. Ritter [d]

[a] Department of Chemistry, Moscow State University, Leninskie Gory, House 1, Building 3, Gsp-2, Moscow 119992, Russia
[b] Department of Chemistry, McMaster University, 1280 Main Street West, Hamilton, Ontario, Canada L8S 4M1
[c] Indian Institute of Technology Madras, Chennai 600 036, India
[d] Institute Laue-Langevin, 6 Rue J. Horowitz, 38042 Grenoble, France
[e] Institut Néel du CNRS/Université J.Fourier, BP166X, 38042 Grenoble, France
[f] Dipartimento di Chimica, Universita di Genova, Via Dodecaneso 31, 16146 Genova, Italy
[g] LAMIA Laboratory-CNR-INFM, Corso Perrone 24, 16152 Genova, Italy

ARTICLE INFO

Article history:
Received 29 October 2009
Received in revised form
22 March 2010
Accepted 4 April 2010
Available online 9 April 2010

Keywords:
Rare earth intermetallics
Magnetically ordered materials
Magnetocaloric effect
Neutron diffraction

ABSTRACT

The magnetic structure of the Fe_2P-type R_6CoTe_2 phases (R=Gd–Er, space group $P\bar{6}2m$) has been investigated through magnetization measurement and neutron powder diffraction. All phases demonstrate high-temperature ferromagnetic and low-temperature transitions: T_C=220 K and T_{CN}=180 K for Gd_6CoTe_2, T_C=174 K and T_{CN}=52 K for Tb_6CoTe_2, T_C=125 K and T_{CN}=26 K for Dy_6CoTe_2, T_{CN}=60 K and T_N=22 K for Ho_6CoTe_2 and $T_{CN}\sim$30 K and $T_N\sim$14 K for Er_6CoTe_2.

Between 174 and 52 K Tb_6CoTe_2 has a collinear magnetic structure with $\mathbf{K}_0$=[0, 0, 0] and with magnetic moments along the c-axis, whereas below 52 K it adopts a non-collinear ferromagnetic one.

Below 60 K the magnetic structure of Ho_6CoTe_2 is that of a non-collinear ferromagnet. The holmium magnetic components with a $\mathbf{K}_0$=[0, 0, 0] wave vector are aligned ferromagneticaly along the c-axis, whereas the magnetic component with a $\mathbf{K}_1$=[1/2, 1/2, 0] wave vector are arranged in the ab plane. The low-temperature magnetic transition at $\sim$22 K coincides with the reorientation of the Ho magnetic component with the $\mathbf{K}_0$ vector from the collinear to the non-collinear state.

Below 30 K Er_6CoTe_2 shows an amplitude-modulate magnetic structure with a collinear arrangement of magnetic components with $\mathbf{K}_0$=[0, 0, 0] and $\mathbf{K}_1$=[1/2, 1/2, 0]. The low-temperature magnetic transition at $\sim$14 K corresponds to the variation in the magnitudes of the M_{Er}^{K0} and M_{Er}^{K1} magnetic components.

In these phases, no local moment was detected on the cobalt site.

The magnetic entropy of Gd_6CoTe_2 increases from $\Delta S_{mag}=-4.5$ J/kg K at 220 K up to $\Delta S_{mag}=-6.5$ J/kg K at 180 K for the field change $\Delta\mu_0 H$=0–5 T.

1. Introduction

The R_6TX_2 phases (R=Gd–Tm, T=Mn, Fe, Co, Ni, Ru and X=Sb, Bi, Te) are known to adopt a Fe_2P-type structure (space group $P\bar{6}2m$, no. 189) [1–4]. In the Fe_2P-type structure, the R atoms occupy the 3(g) site (X_{R1}, 0, 1/2) and 3(f) site (X_{R2}, 0, 0), transition metal atoms occupy the special position 1(b) (0, 0, 1/2) and antimony (bismuth, tellurium) atoms occupy the special position 2(c) (1/3, 2/3, 0) (Fig. 1a). As a rule, the rare earth Fe_2P-type compounds demonstrate two ferromagnetic transitions: into a high-temperature collinear ferromagnetic state (Tb_6FeBi_2, Er_6{Mn, Fe}Sb_2, Er_6MnBi_2, Ho_6FeSb_2, Ho_6FeBi_2 and Ho_6MnBi_2) and into a low-temperature non-collinear ferromagnetic state (Tb_6FeBi_2, Ho_6FeSb_2, Ho_6FeBi_2 and Ho_6MnBi_2 [5–7]). Ho_6CoBi_2 shows a high-temperature collinear ferromagnetic ordering, too, but the low-temperature ferromagnetic one has a wave vector $\mathbf{K}$=[0, 0, ±1/5] [7]. No local moment was detected on the transition metal site. Both the type of the transition metal and the distortion of the unit cell strongly influence the magnetic ordering temperature and hence the magnetic structure in these compounds. The Mn-containing phases show highest magnetic ordering temperature among the whole series.

Magnetocaloric properties have been investigated for Tb_6FeSb_2 and Tb_6FeBi_2 [8]. The Tb_6FeSb_2 has a magnetic entropy change $\Delta S_{mag}=-2.24$ J/kg K at T_C=256 K for the field change ΔH=0–2 T, whereas Tb_6FeBi_2 shows $\Delta S_{mag}=-2.56$ J/kg K at T_C=246 K for ΔH=0–2 T [8].

To understand the effect of transition metal and p-element atoms on the magnetic properties of R_6TX_2, the magnetic structure of the R_6CoTe_2 phases has been investigated through the combination of magnetization measurement and neutron powder diffraction.

* Corresponding author.
E-mail address: morozkin@general.chem.msu.ru (A.V. Morozkin).

0022-4596/$ - see front matter © 2010 Elsevier Inc. All rights reserved.
doi:10.1016/j.jssc.2010.04.002

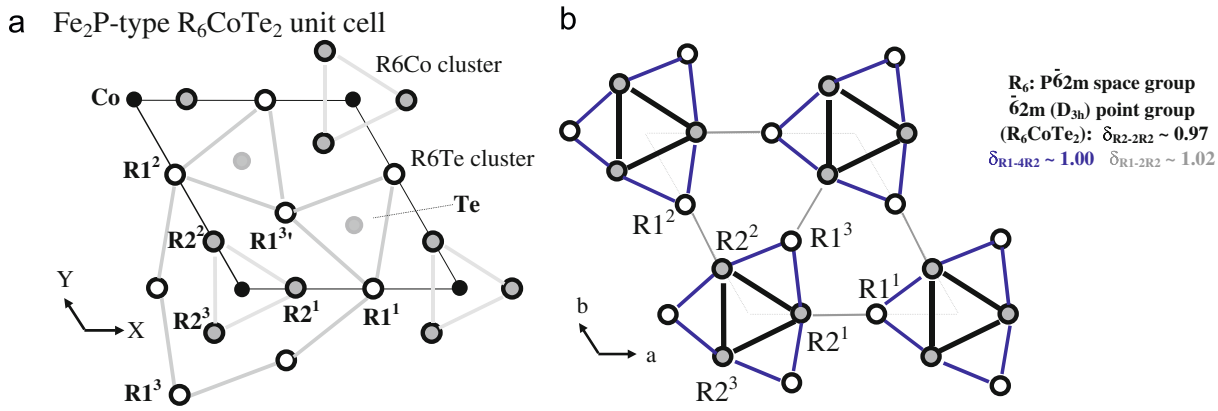

Fig. 1. Unit cell of Fe_2P-type R_6CoTe_2 (a) and rare earth sublattice in Fe_2P-type unit cell with the *R*2–2*R*2, *R*1–4*R*2 and *R*1–2*R*2 shortest bonds indicated (b).

Table 1
Crystallographic data and magnetic properties of the Fe_2P-type R_6CoTe_2 compounds (space group $P\bar{6}2m$ No. 189, atomic sites: R_1 3(*g*) [X_{R1}, 0, 1/2], R_2 3(*f*) [X_{R2}, 0, 0], Co 1(b) [0, 0, 1/2], *X* 2(*c*) [1/3, 2/3, 0]).

Compound	Unit cell data at 300 K	Atomic positions at 300 K	R_F (%)	T_{CN} (K) (H=0.01 T)	M_{sat}/R (μ_B)	ΔS_{magn} (J/kg K)	T_m^{ND} (K)	Magnetic structure [e]
Sc_6CoTe_2 [a]	a=0.78209 nm [b] c=0.37995 nm							
Y_6CoTe_2 [a]	a=0.82479 nm [b] c=0.39402 nm							
Gd_6CoTe_2 [4]	a=0.8378(1) nm c=0.39831(5) nm	X_{Gd1}=0.589(1) X_{Gd2}=0.241(1)	5.9	T_C=220 K T_{CN}=180 K	3.94 (184 K, 5 T)	−4.5 (5 T) −6.5 (5 T)		
Tb_6CoTe_2	a=0.83087(4) nm c=0.39627(2) nm	X_{Tb1}=0.5975(3) X_{Tb2}=0.2382(3)	3.8				$T_C=T_{m1}^{ND}$=174 K $T_{CN}=T_{m2}^{ND}$=52 K	F {$M_{(Tb1,\ Tb2)c}^{K0}$ (3m) F {$M_{(Tb1,\ Tb2)c}^{K0}$ (3*m*)+ +(F–AF)$M_{(Tb1,\ Tb2)ab}^{K0}$ (m_h)
Dy_6CoTe_2	a=0.82698(9) nm c=0.39493(3) nm	X_{Dy1}=0.5947(8) X_{Dy2}=0.2407(8)	4.6	T_C=125 K T_{CN}=26 K				
Ho_6CoTe_2 [c]	a=0.82328(2) nm c=0.39352(1) nm	X_{Ho1}=0.6001(2) X_{Ho2}=0.2376(2)	3.4	T_{CN}=60 K T_N~22 K			T_{m1}^{ND}~60 K T_{m2}^{ND}~22 K	F {$M_{(Ho1,\ Ho2)c}^{K0}$ (3*m*)+ +AF {$M_{(Ho1,\ Ho2)ab}^{K1}$ ($m'm_h$) F {$M_{(Ho1,\ Ho2)c}^{K0}$ (3*m*)+ +AF {$M_{(Ho1,\ Ho2)ab}^{K1}m'm_h$)+ +(F–AF) {$M_{(Ho1,\ Ho2)ab}^{K0}$ (m_h)
Er_6CoTe_2	a=0.81950(5) nm c=0.39228(2) nm	X_{Er1}=0.5977(4) X_{Er2}=0.2373(4)	4.7				$T_{CN}=T_{m1}^{ND}$=30 K $T_N=T_{m2}^{ND}$~14 K	AF {$M_{(Er1,\ Er2)ab}^{K1}$ (2mm_h) + +(F–AF) {$M_{(Er1,\ Er2)ab}^{K0}$ (m_h) AF {$M_{(Er1,\ Er2)ab}^{K1}$ (2mm_h)+ +(F–AF) {$M_{(Er1,\ Er2)ab}^{K0}$ (m_h)
Tm_6CoTe_2 [a]	a=0.81503 nm [b] c=0.39081 nm			T_C~16 K [d]				
Lu_6CoTe_2 [a]	a=0.81015 nm [b] c=0.38920 nm							

[a] Hypothetical compounds.
[b] Hypothetical lattice parameters as deduced from atomic radii rule–see Fig. 2.
[c] The crystallographic data for Ho_6CoTe_2 used with permission—© JCPDS–International Centre for Diffraction Data.
[d] Hypothetical from de Gennes rule.
[e] F the ferromagnetic component; (F–AF) the ferromagnetic with antiferromagnetic component (non-collinear ferromagnetic); AF the antiferromagnetic component of {$M_{(R1,\ R2)ab}^{K0,\ K1}$}{$M_{(R1,\ R2)c}^{K0}R$} atoms in the *ab* plane ore along *c*-axis with corresponding wave vectors $\mathbf{K}_0$=[0, 0, 0], $\mathbf{K}_1$=[1/2, 1/2, 0] and corresponding magnetic point group (3*m*), (2mm_h), ($m'm_h$) and (m_h).

2. Experimental details

The phases under discussion were prepared by arc-melting in an electric arc furnace under an argon atmosphere using a non-consumable tungsten electrode and a water-cooled copper tray. Pieces of tellurium (purity 99.99 wt%), gadolinium, terbium, holmium, erbium and cobalt (99.9 wt% purity for all of the elements) were used as the starting components. Titanium was

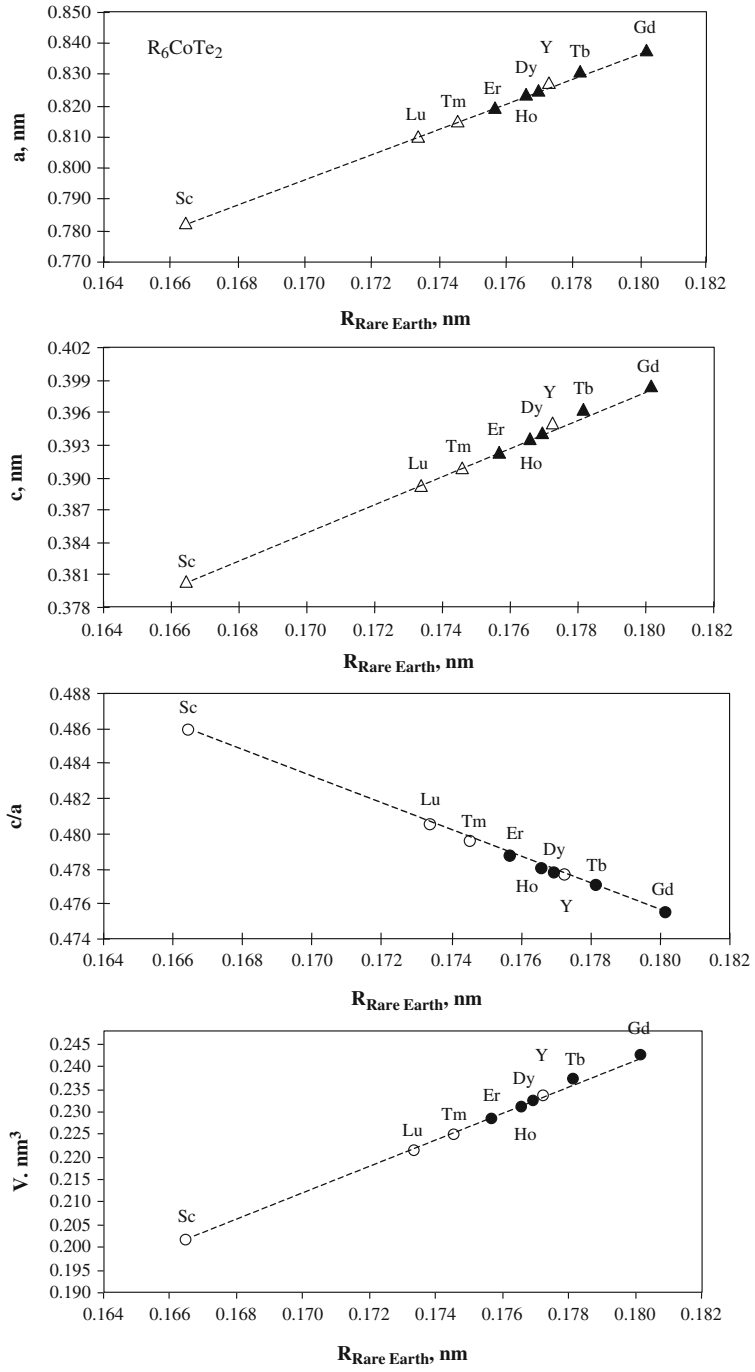

Fig. 2. Cell parameters vs. atomic radii ($R_{\text{Rare Earth}}$) of rare earths for the of R_6CoTe_2 phases. The open symbols correspond to the lattice parameters of hypothetical compounds not studied here but whose lattice parameters are deduced from the general trend of the lanthanide contraction. The error bars are smaller than the corresponding symbols.

Table 2
Interatomic distances in Ho_6CoTe_2 and their ratio to the sum of the corresponding atomic radii $\delta = D/(R_{\text{atomic1}} + R_{\text{atomic2}})$.

Atom1–Atom2	D (nm)	δ	Coordination number	Atom1–Atom2	D (nm)	δ	Coordination number
Ho1–4Te	0.31936	1.00	13	Co–6Ho2	0.27745	0.92	11
–1Co	0.32923	1.09		–3Ho1	0.32293	1.09	
–4Ho2	0.34781	1.00		–2Co	0.39352	1.58	
–2Ho2	0.35746	1.02					
–2Ho1	0.39352	1.13		Te–3Ho2	0.32117	1.00	11
Ho2–2Co	0.27745	0.92	14	–6Ho1	0.31936	1.00	
–2Te	0.32117	1.00		–2Te	0.39352	1.37	
–2Ho2	0.33881	0.97					
–4Ho1	0.34781	1.00					
–2Ho1	0.35746	1.02					
–2Ho2	0.39352	1.13					

used as a getter during arc-melting. The arc-melted samples were annealed at 1070 K for 200 h in an argon atmosphere and quenched in ice-cold water.

The quality of the samples before the neutron diffraction study was evaluated using X-ray diffraction and electron microprobe analysis. The X-ray data were obtained on a diffractometer DRON-3.0 (Cu$K\alpha$ radiation, $2\Theta = 5$–120°, step 0.02°, 10 s per step). The lattice constants were derived using the Rietan-program [9] in the isotropic approximation (Table 1). A "Camebax" microanalyser was employed to perform microprobe X-ray spectral analyses of the samples.

The neutron diffraction studies were carried out on the powder D1B diffractometer [10] (Institute Laue-Langevin, Grenoble, France) from 290 to 2 K for Tb_6CoTe_2, from 80 K down to 2 K for Ho_6CoTe_2 and from about 40 K down to 2 K for Er_6CoTe_2 (temperature step 1–5 K). The neutron diffraction data were analyzed and refined using the FULLPROF98-program in terms of traditional crystallographic approach [11].

The dc magnetization was measured with use of a commercial SQUID magnetometer (Quantum Design) in the temperature range of 5–300 K in the applied field up to 5 T.

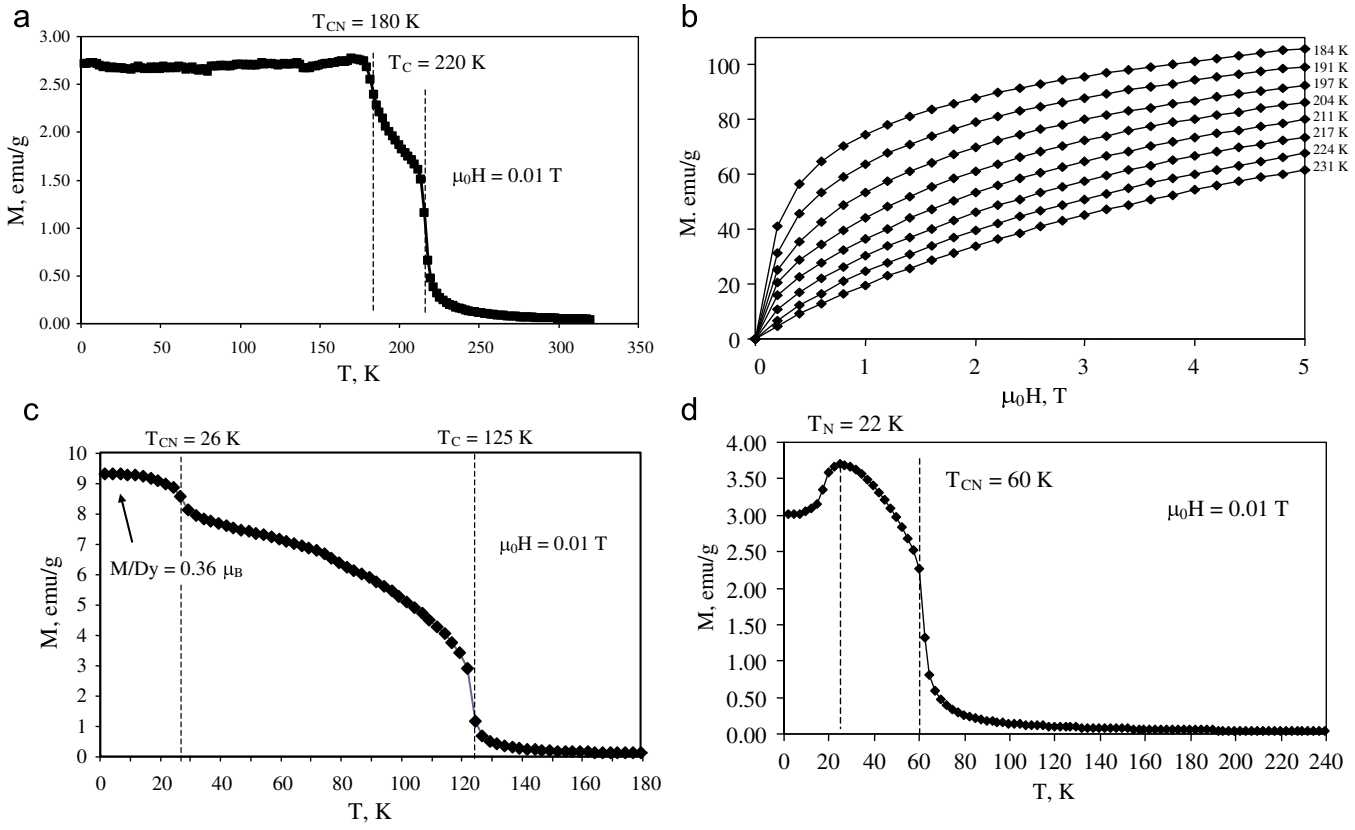

Fig. 3. (a) Magnetization vs. temperature and (b) vs. magnetic field around the magnetic transitions for Gd_6CoTe_2. Magnetization vs. temperature for Dy_6CoTe_2 (c) and Ho_6CoTe_2 (d).

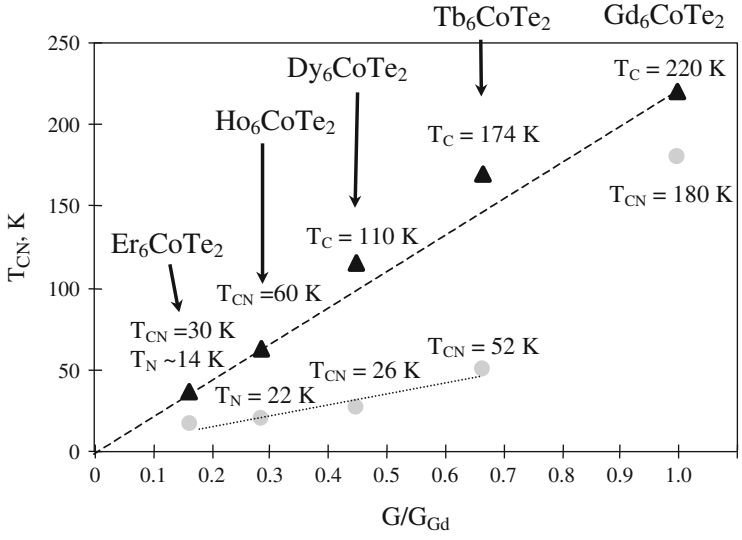

Fig. 4. Magnetic transition temperatures vs. de Gennes factor for R_6CoTe_2.

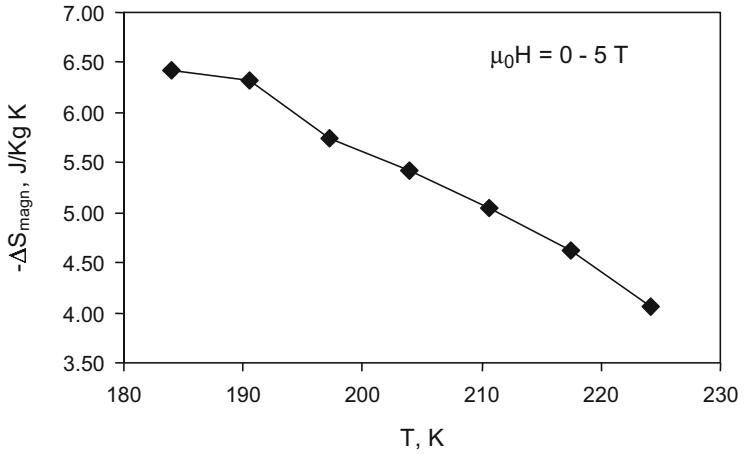

Fig. 5. The isothermal entropy change, ΔS_{magn}, of Gd_6CoTe_2 between the high-temperature, T_C=220 K, and low-temperature, T_{CN}=180 K, magnetic transitions.

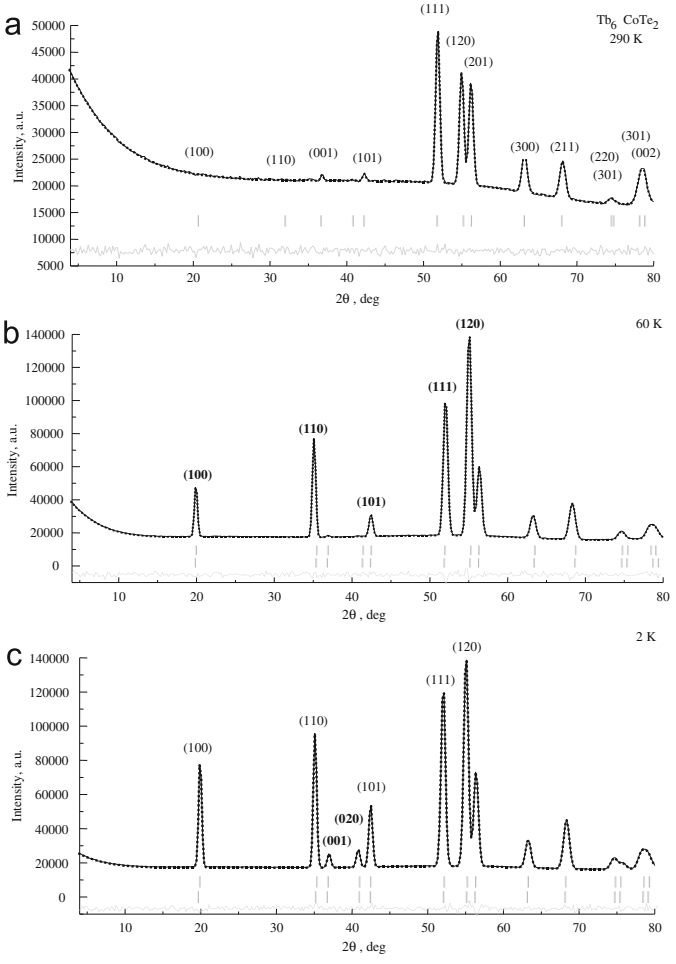

Fig. 6. Neutron diffraction pattern of Tb_6CoTe_2 at (a) 290 K (paramagnetic state), (b) 60 K (collinear ferromagnetic) and (c) 2 K (non-collinear ferromagnetic) with λ=0.254 nm.

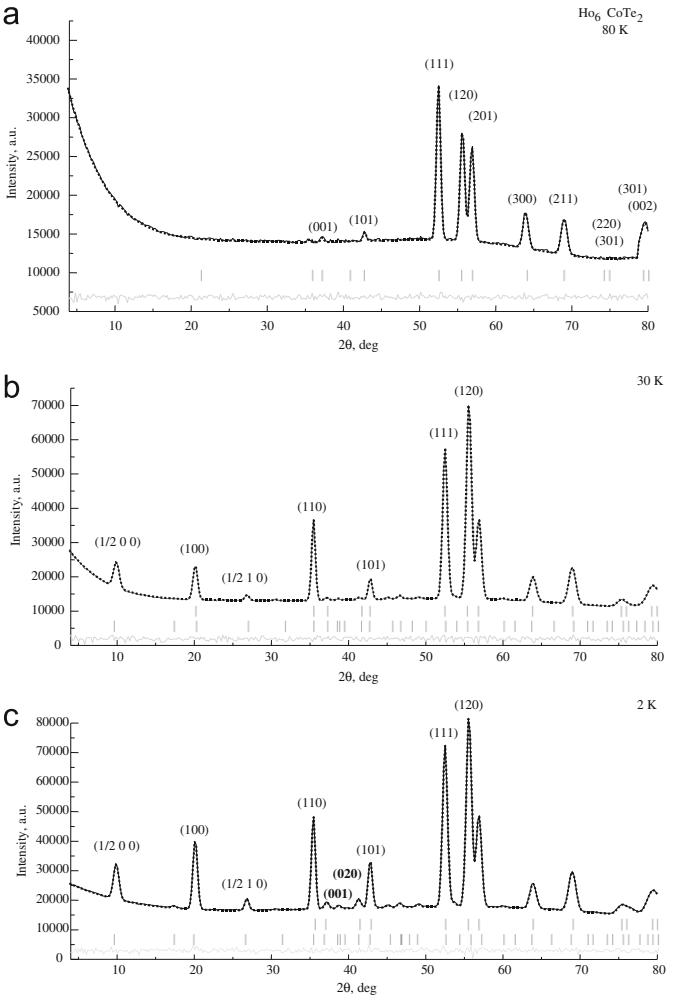

Fig. 7. Neutron diffraction pattern of Ho_6CoTe_2 at (a) 80 K (paramagnetic state), (b) 30 K (non-collinear ferromagnetic) and (c) 2 K (non-collinear ferromagnetic) with λ=0.254 nm.

3. Results and discussion

3.1. Crystal structure

The structure of the Fe_2P-type R_6CoTe_2 compounds projected onto the *ab* plane is shown in Fig. 1a. The Fe_2P-type R_6CoTe_2 lattice contains the Co and Te sublattices with the $6/m$ (D_{6h}) point group and the rare-earth sublattice with the $\bar{6}2m$ (D_{3h}) point group ($P\bar{6}2m$ space group). The rare-earth atoms occupy the following positions: $R1^1$ (X_{R1}, 0 1/2), $R1^2$ (0, X_{R1}, 1/2), $R1^3$ ($-X_{R1}$, $-X_{R1}$, 1/2); $R2^1$ (X_{R2}, 0, 0), $R2^2$ (0, X_{R2}, 0) and $R2^3$ ($-X_{R2}$, $-X_{R2}$, 0). The shortest *R*1–Te, *R*2–Te, *R*1–*R*2 interatomic distances are close to the sum of metallic radii of pure elements, whereas the *R*2–Co and *R*2–*R*2 interatomic distances are less than the sum of metallic

radii [12]. The interatomic distances for Ho_6CoTe_2 are summarized in Table 2. The rare-earth atoms form the semi-isolated cluster with the $\bar{6}2m$ (D_{3h}) point group that are shown in Fig. 1b.

The *a*, *c* cell parameters and the volume of the unit cell, *V*, of the R_6CoTe_2 phases increase with the size of rare-earth atoms, whereas the *c*/*a* ratio shows the opposite trend (Fig. 2). The *a* and *c* parameters for the hypothetical Sc_6CoTe_2, Y_6CoTe_2, Tm_6CoTe_2 and Lu_6CoTe_2 phases with the same structure were extracted from the extrapolation of the corresponding linear fits (Table 1 and Fig. 2).

3.2. Magnetization

Magnetization measurements indicate two magnetic transitions for Gd_6CoTe_2, Dy_6CoTe_2 and Ho_6CoTe_2 (Table 1 and Fig. 3). The high-temperature magnetic transitions are associated with the ferromagnetic ordering, and the low-temperature ones may correspond to the reorientation of magnetic moments and appearance of antiferromagnetic components in the ferromagnetic system. The temperature of the ferromagnetic transitions in Gd_6CoTe_2, Dy_6CoTe_2 and Ho_6CoTe_2 follows the de Gennes rule (Fig. 4). The temperature of the magnetic ordering in Tm_6CoTe_2 is estimated from de Gennes rule (Table 1).

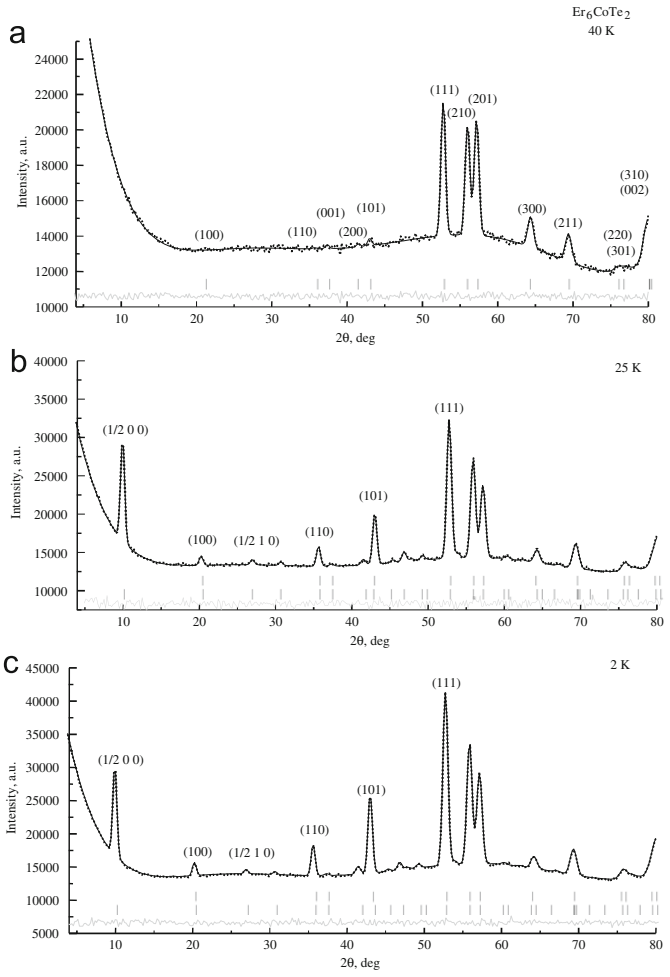

Fig. 8. Neutron diffraction pattern of Er_6CoTe_2 at (a) 40 K (paramagnetic state), (b) 25 K (amplitude-modulated ferromagnetic) and (c) 2 K (amplitude-modulated ferromagnetic) with $\lambda = 0.254$ nm.

3.3. Magnetocaloric effect

The magnetocaloric effect for Gd_6CoTe_2 was evaluated from the magnetization vs. field (*M* vs. *H*) data measured around the Curie temperatures with 7 K increments. The magnetic field changed from 0 to 5 T in 0.2 T steps. MCE in terms of the isothermal entropy change, ΔS, was calculated from the magnetization data (Fig. 5) through the Maxwell equation [13]: $\left(\partial S(T,H)/\partial H\right)_T = \left(\partial M(T,H)/\partial T\right)_H$. Through the integration of the partial derivative of magnetization, *M*, with respect to temperature, *T*, over a change in the magnetic field, *H*, expression for the ΔS is obtained as: $\Delta S(T)_{\Delta H} = \int_{H_1}^{H_2}\left(\partial M(T,H)/\partial T\right)_{H,p} dH$. In practice a numerical integration is performed using the following formula: $\Delta S(T)_{\Delta H} = \sum_i((M_{i+1}-M_i)/(T_{i+1}-T_i))\Delta H$, where ΔH is a change in magnetic

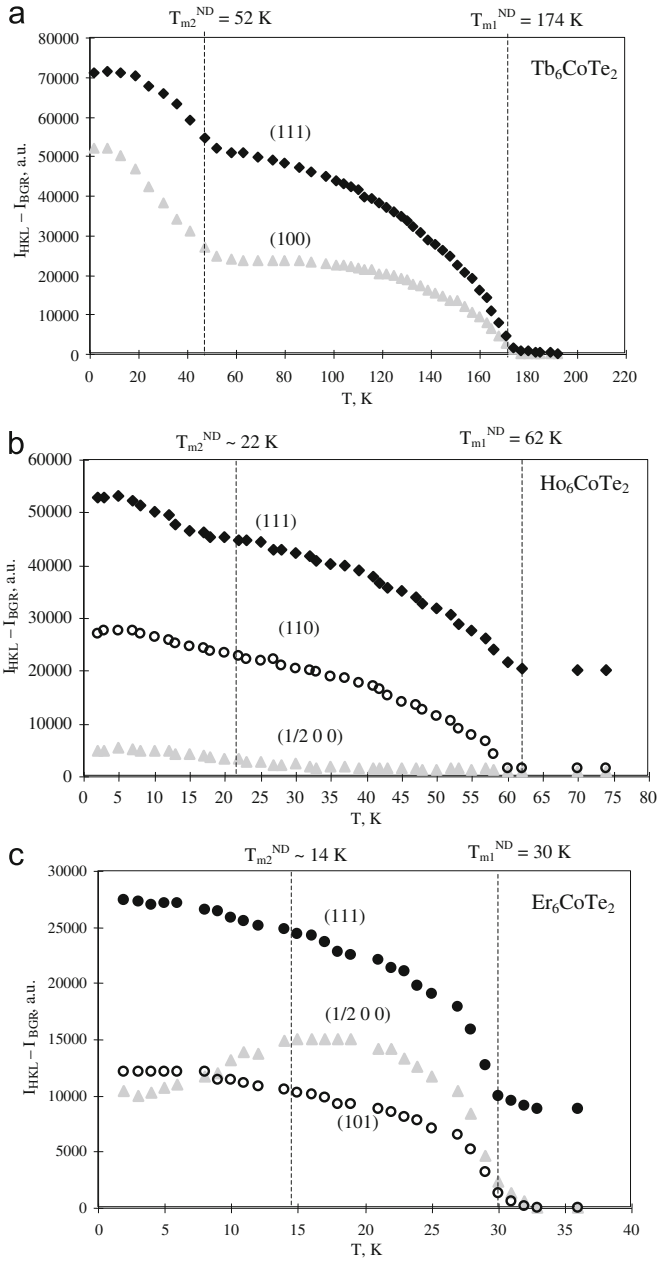

Fig. 9. Thermal variation of intensity of magnetic reflections in (a) Tb_6CoTe_2, (b) Ho_6CoTe_2 and (c) Er_6CoTe_2.

field and M_i and M_{i+1} are the values of magnetization at temperatures T_i and T_{i+1}, respectively.

The magnetocaloric effect for Gd_6CoTe_2 in terms of the isothermal entropy change, ΔS_{magn}, increases from the high-temperature to low-temperature magnetic transition (Fig. 5). The maximum $|\Delta S_{magn}|$ value is close to the values observed for isostructural Tb_6FeSb_2 and Tb_6FeBi_2 [8] but less than for pure Gd ($-\Delta S_{mag}$/molGd$\sim$1 J/mol K for Gd_6CoTe_2 at 180 K for $\Delta\mu_0 H=0-5$ T and $-\Delta S_{mag}$/molGd=1.54 J/mol K for pure Gd at 293 K for $\Delta\mu_0 H=0-5$ T [14]).

3.4. Neutron diffraction study

3.4.1. Magnetic transitions

Figs. 6–8 show the neutron diffraction patterns recorded at different temperatures in zero applied magnetic field for Tb_6CoTe_2, Ho_6CoTe_2 and Er_6CoTe_2. No incommensurate magnetic reflections were detected in Tb_6CoTe_2, whereas both commensurate magnetic reflections with $\mathbf{K}_0=[0, 0, 0]$ and with incommensurate $\mathbf{K}_1=[1/2, 1/2, 0]$ were observed for Ho_6CoTe_2 and Er_6CoTe_2. Thermal variations in the intensities of the magnetic reflections indicate magnetic transitions at 174 and 52 K for Tb_6CoTe_2, at 60 and 22 K for Ho_6CoTe_2 and at 30 and $\sim$14 K for Er_6CoTe_2 (Fig. 9).

3.4.2. Magnetic structure

The $\bar{6}2m$ (D_{3h}) point group consists of invariant $3m$ (C_{3v}) subgroup and ($m_h\times 3m$) subgroup of index 2. The possible magnetic point groups for the $\bar{6}2m$ (D_{3h}) point group of the rare-earth sublattice of the Fe_2P-type phases are "colourless" $\bar{6}2m$ (D_{3h}), $\bar{6}(3/m_h)$ (C_{3h}), $3m$ (C_{3v}), $2mm_h$ (D_{1h}), m (C_{1v}), m_h (C_{1h}) and trivial 1 (C_1) and "black-white" (Shubnikov) $3m'$ and m' ($m'm_h$) [15].

The $\bar{6}2m$ ($3mm_h$) (D_{3h}), $\bar{6}$ ($3/m_h$) (C_{3h}), $2mm_h$ (D_{1h}), m_h (C_{1h}) and $m'm_h$ magnetic point groups correspond to the *ab*-oriented magnetic ordering, whereas the $3m$, $3m'$, m and m' magnetic point groups correspond to the ordering of the rare-earth magnetic moments along the *c*-axis in the Fe_2P-type phases.

The magnetic structures of the R_6CoTe_2 phases were determined in terms of the above-mentioned magnetic point groups in association with the translation group in case of the commensurate magnetic component ($\mathbf{K}_0=[0, 0, 0]$) and with the translation/antitranslation group in case of the incommensurate magnetic component ($\mathbf{K}_1=[1/2,1/2,0]$).

The evolution of the magnetic order upon cooling can be clearly identified from the development of magnetic reflections for Tb_6CoTe_2, Ho_6CoTe_2 and Er_6CoTe_2 (Figs. 6–8). Magnetic structures and temperatures of magnetic transition were determined form the refinements of neutron powder diffraction data. The crystallographic and magnetic parameters for Tb_6CoTe_2, Ho_6CoTe_2 and Er_6CoTe_2 are summarized in Tables 3–5. Refined values of the rare earth magnetic moments have to be compared to the theoretical values of the Tb, Ho and Er ions ($M_{Tb3+}=9\,\mu_B$, $M_{Ho3+}=10\,\mu_B$ and $M_{Er3+}=9\,\mu_B$) in the trivalent state [16].

3.4.2.1. Tb_6CoTe_2. Below 174 K, Tb_6CoTe_2 has a collinear magnetic structure with the $3m$ magnetic point group for the Tb sublattice (the Tb magnetic moments are ferromagnetically ordered along the *c*-axis) (Fig. 10a): $\{M^{K0}_{(Tb1,\ Tb2)c}\}$ ($3m$). The magnetic moments of Tb1 and Tb2 have strongly different values (Table 3).

Below 52 K the Tb_6CoTe_2 magnetic structure becomes a non-collinear ferromagnet due to the presence of magnetic point group m_h for the *ab* components (Fig. 10b): $\{M_{(Tb1,\ Tb2)abc}{}^{K0}\}$ (1)=$\{M_{(Tb1,\ Tb2)c}{}^{K0}\}$ ($3m$)+$\{M_{(Tb1,\ Tb2)ab}{}^{K0}\}$ (m_h). The models with the another magnetic point groups had no satisfactory agreement with the experimental data. The magnetic structure projected onto the *ab* plane consists of collinear, ferromagnetically ordered domains (Fig. 10b).

The symmetry of the high-temperature magnetic ordering closes the symmetry of the rare-earth sublattice, whereas the low-temperature magnetic ordering leads to a decrease in the magnetic symmetry.

The thermal variation of the terbium magnetic moments and their angles around the *c*-axis are shown in Figs. 11a and b. Details of the Tb_6CoTe_2 magnetic structure are given in Table 3.

Table 3.
Crystallographic and magnetic parameters at different temperature *T* (K) for Tb_6CoTe_2. T_m^{Neu} (K) is the transition temperature from the neutron diffraction study; "Para" is for the paramagnetic state, "F" is for the ferromagnetic state, "F-AF" is for the ferromagnet with an antiferromagnetic component; $\{M_{(Tb1,\ Tb2)c}\}$ and $\{M_{(Tb1,\ Tb2)ab}\}$ is the set of magnetic components of Tb1 and Tb2 atoms along *c*-axis ore in the *ab* plane, ($3m$) and (1) are the point group of these components, X_{Tb1} and X_{Tb2} are the atomic parameters, M_j^{K0} (μ_B) is the magnitude of magnetic moment with the wave vectors $\mathbf{K}_0=[0, 0, 0]$; φ_j^{K0} and θ_j^{K0} are the angles (deg) of the corresponding magnetic moments with the *a* and *c* axes, respectively.

T_m^{Neu}	Type	*T*	Unit cell data	R_F (%)	Atom	M_j^{K0}	φ_j^{K0}	θ_j^{K0}	R_F^m (%)
	Para	300[a]	$a=0.83087(4)$ nm $c=0.39627(2)$ nm $X_{Tb1}=0.5975(3)$ $X_{Tb2}=0.2382(3)$	3.8					
	Para	290	$a=0.8312(4)$ nm $c=0.3970(2)$ nm $X_{Tb1}=0.591(1)$ $X_{Tb2}=0.239(1)$	3.9					
174	F $\{M_{(Tb1,\ Tb2)c}{}^{K0}\}$ ($3m$)	58	$a=0.8299(1)$ nm $c=0.39548(7)$ nm $X_{Tb1}=0.592(1)$ $X_{Tb2}=0.2405(7)$	3.5	Tb1[1] Tb1[2] Tb1[3] Tb2[1] Tb2[2] Tb2[3]	5.7(2) 5.7(2) 5.7(2) 9.0(2) 9.0(2) 9.0(2)	0 0 0 0 0 0	0 0 0 0 0 0	1.7
52	F $\{M_{(Tb1,\ Tb2)c}{}^{K0}\}$ ($3m$)+(F–AF)$\{M_{(Tb1,\ Tb2)ab}{}^{K0}m_h\}$	2	$a=0.8299(1)$ nm $c=0.39506(5)$ nm $X_{Tb1}=0.594(1)$ $X_{Tb2}=0.2412(8)$	1.8	Tb1[1] Tb1[2] Tb1[3] Tb2[1] Tb2[2] Tb2[3]	8.1(2) 8.1(2) 8.1(2) 9.0(2) 9.0(2) 9.0(2)	315 45 45 45 315 315	52(1) 52(1) 52(1) 14(1) 14(1) 14(1)	2.0

[a] X-ray data.

Table 4.
Crystallographic and magnetic parameters at different temperature T (K) for Ho_6CoTe_2. T_{CN} (K) and T_m^{Neu} (K) are the transition temperatures from the magnetization and neutron diffraction studies; "Para" is for the paramagnetic state, "F" and "AF" is for the ferromagnetic and antiferromagnetic component, "F–AF" is for the ferromagnet with an antiferromagnetic component; $\{M_{(Ho1,\ Ho2)c}\}$ and $\{M_{(Ho1,\ Ho2)ab}\}$ are the set of magnetic components of Ho1 and Ho2 atoms along c-axis or in the ab plane, $(3m)$, (m') and (1) are the point group of these components; X_{Ho1} and X_{Ho2} are the atomic parameters, M_j^{K0} and M_j^{K1} (μ_B) are the magnitudes of magnetic moments with the wave vectors $\mathbf{K}_0=[0, 0, 0]$ and $\mathbf{K}_1=[1/2, 1/2, 0]$; φ_j^{Ki} and θ_j^{Ki} are the angles (deg) of the corresponding magnetic moments with the a and c axes, respectively.

T_{CN}	T_m^{Neu}	Type	T	Unit cell data	R_F (%)	Atom	M_j^{K0}	φ_j^{K0}	θ_j^{K0}	M_j^{K1}	φ_j^{K1}	θ_j^{K1}	R_F^m (%)
		Para	300[a]	$a=0.82328(2)$ nm $c=0.39352(1)$ nm $X_{Ho1}=0.6001(2)$ $X_{Ho2}=0.2376(2)$	4.7								
		Para	80	$a=0.8227(4)$ nm $c=0.3928(2)$ nm $X_{Ho1}=0.597(1)$ $X_{Ho2}=0.238(2)$	3.3								
60	~60	$FM_{(Ho1,\ Ho2)c}{}^{K0}$ $(3m)$ $AFM_{(Ho1,\ Ho2)ab}{}^{K1}(m'm_h)$	25	$a=0.8233(2)$ nm $c=0.3925(1)$ nm $X_{Ho1}=0.596(1)$ $X_{Ho2}=0.239(7)$	2.6	$Ho1^1$ $Ho1^2$ $Ho1^3$ $Ho2^1$ $Ho2^2$ $Ho2^3$	4.4(2) 4.4(2) 4.4(2) 7.7(2) 7.7(2) 7.7(2)	0 0 0 0 0 0	0 0 0 0 0 0	1.50(6) 1.50(6) 1.50(6) 1.50(6) 1.50(6) 1.50(6)	60 240 60 60 240 240	90 90 90 90 90 90	6.0
22	~22	$FM_{(Ho1,\ Ho2)c}{}^{K0}$ $(3m)$ $AFM_{(Ho1,\ Ho2)ab}{}^{K1}(m'm_h)$ $F\text{-}AFM_{(Ho1,\ Ho2)ab}{}^{K0}$ (m_h)	2	$a=0.8231(2)$ nm $c=0.3924(1)$ nm $X_{Ho1}=0.596(2)$ $X_{Ho2}=0.240(1)$	2.4	$Ho1^1$ $Ho1^2$ $Ho1^3$ $Ho2^1$ $Ho2^2$ $Ho3^3$	4.9(2) 4.9(2) 4.9(2) 7.4(2) 7.4(2) 7.4(2)	15 15 15 105 105 105	52(2) 52(2) 52(2) 22(2) 22(2) 22(2)	1.63(6) 1.63(6) 1.63(6) 1.63(6) 1.63(6) 1.63(6)	60 240 60 60 60 60	90 90 90 90 90 90	6.0

[a] X-ray data.

Table 5.
Crystallographic and magnetic parameters at different temperatures T (K) for Er_6CoTe_2. T_m^{Neu} (K) is the transition temperature from the neutron diffraction study; "Para" is for the paramagnetic state, "AF" is for the antiferromagnetic component, "F–AF" is for the ferromagnet with an antiferromagnetic component); $\{M_{(Er1,\ Er2)ab}\}$ is the set of magnetic components of Er1 and Er2 atoms in the ab plane, (m) and (1) are the point group of these components; X_{Er1} and X_{Er2} are the atomic coordinates, M_j^{K0} and M_j^{K1} (μ_B) are the magnitude of magnetic moment with the wave vectors $\mathbf{K}_0=[0, 0, 0]$ and $\mathbf{K}_1=[1/2, 1/2, 0]$; φ_j^{Ki} and θ_j^{Ki} are the angles (deg) of the corresponding magnetic moments with the a and c axes, respectively.

T_m^{Neu}	Type	T	Unit cell data	R_F (%)	Atom	M_j^{K0}	φ_j^{K0}	θ_j^{K0}	M_j^{K1}	φ_j^{K1}	θ_j^{K1}	R_F^m (%)
	Para	300[a]	$a=0.81950(5)$ nm $c=0.39228(2)$ nm $X_{Er1}=0.5977(4)$ $X_{Er2}=0.2373(4)$	4.7								
	Para	40	$a=0.8183(4)$ nm $c=0.3914(2)$ nm $X_{Er1}=0.580(2)$ $X_{Er2}=0.240(2)$	7.6								
30	$F\text{–}AFM_{(Er1,\ Er2)ab}{}^{K0}$ (m_h) $AFM_{(Er1,\ Er2)ab}{}^{K1}(2mm_h)$	20	$a=0.8194(4)$ nm $c=0.3906(2)$ nm $X_{Er1}=0.583(2)$ $X_{Er2}=0.234(2)$	3.6	$Er1^1$ $Er1^2$ $Er1^3$ $Er2^1$ $Er2^2$ $Er2^3$	6.6(2) 4.4(2) 4.4(2) 6.6(2) 6.6(2) 6.6(2)	60 60 60 60 60 60	90 90 90 90 90 90	2.05(8) 2.05(8) 2.05(8) 2.05(8) 2.05(8) 2.05(8)	60 60 240 240 240 240	90 90 90 90 90 90	7.8
14	$F\text{–}AFM_{(Er1,\ Er2)ab}{}^{K0}$ (m_h) $AFM_{(Er1,\ Er2)ab}{}^{K1}(2mm_h)$	2	$a=0.8194(4)$ nm $c=0.3907(2)$ nm $X_{Er1}=0.584(2)$ $X_{Er2}=0.238(2)$	4.2	$Er1^1$ $Er1^2$ $Er1^3$ $Er2^1$ $Er2^2$ $Er2^3$	7.6(2) 4.6(2) 4.6(2) 4.6(2) 4.6(2) 4.6(2)	60 60 60 60 60 60	90 90 90 90 90 90	1.75(8) 1.75(8) 1.75(8) 1.75(8) 1.75(8) 1.75(8)	60 60 240 240 240 240	90 90 90 90 90 90	8.2

[a] X-ray data.

3.4.2.2. Ho_6CoTe_2. Below 60 K the magnetic structure of Ho_6CoTe_2 is non-collinear ferromagnetic. The holmium magnetic components with a $\mathbf{K}_0=[0, 0, 0]$ wave vector are ferromagneticaly coupled and directed along the c-axis ($\{M_{(Ho1,\ Ho2)c}{}^{K0}\}$ $(3m)$ component) (Fig. 10a). The holmium magnetic component with a $\mathbf{K}_1=[1/2,1/2,0]$ wave vector arranged in the ab plane and belong to the $m'm_h$ point group (Fig. 10c): $\{M_{(Ho1,\ Ho2)ab}{}^{K1}\}$ $(m'm_h)$. The magnetic structure projected onto the ab plane consists of collinear, ferromagnetically ordered domains similar to those in Tb_6CoTe_2 and the magnetic symmetry of Ho_6CoTe_2 is $\{M_{(Ho1,\ Ho2)c}{}^{K0}\}$ $(3m)+\{M_{(Ho1,\ Ho2)ab}{}^{K1}\}$ $(m'm_h)$.

The low-temperature magnetic transition at 22 K coincides with the transformation of the Ho magnetic component with the $\mathbf{K}_0$ vector from a collinear to non-collinear state, like in Tb_6CoTe_2 (Fig. 10b): $\{M_{(Ho1,\ Ho2)c}{}^{K0}\}$ $(3m)+\{M_{(Ho1,\ Ho2)ab}{}^{K0}\}$ $(m_h)=\{M_{(Ho1,\ Ho2)abc}{}^{K0}\}$ (1). The Ho_6CoTe_2 magnetic structure is close to a complex ferromagnetic cone due to an additional $\{M_{(Ho1,\ Ho2)ab}{}^{K0}\}$ (m_h) component. The low-temperature magnetic

structure of Ho_6CoTe_2 became $\{M_{(Ho1,\ Ho2)abc}^{K0}\}$ (1)+$\{M_{(Ho1,\ Ho2)ab}^{K1}\}$ ($m'm_h$).

Both, the high-temperature and low-temperature magnetic structures belong to the 1 point group. The thermal variation of the holmium magnetic moments and their angles around the *c*-axis are shown in Figs. 11c and d. Details of the Ho_6CoTe_2 magnetic structure are given in Table 4.

3.4.2.3. Er_6CoTe_2. Below 30 K Er_6CoTe_2 shows an amplitude-modulated magnetic structure (Figs. 10d, e and Table 5). This magnetic structure consists of collinear Er magnetic components with $\mathbf{K}_0=[0, 0, 0]$ and $\mathbf{K}_1=[1/2,1/2,0]$ vectors: $\{M_{(Er1,\ Er2)ab}^{K0}\}$ (m_h)+$\{M_{(Er1,\ Er2)ab}^{K1}\}$ ($2mm_h$). Thermal variation of the erbium magnetic moments (Fig. 11e) and intensity of magnetic reflections (Fig. 9c) indicate a smooth low-temperature

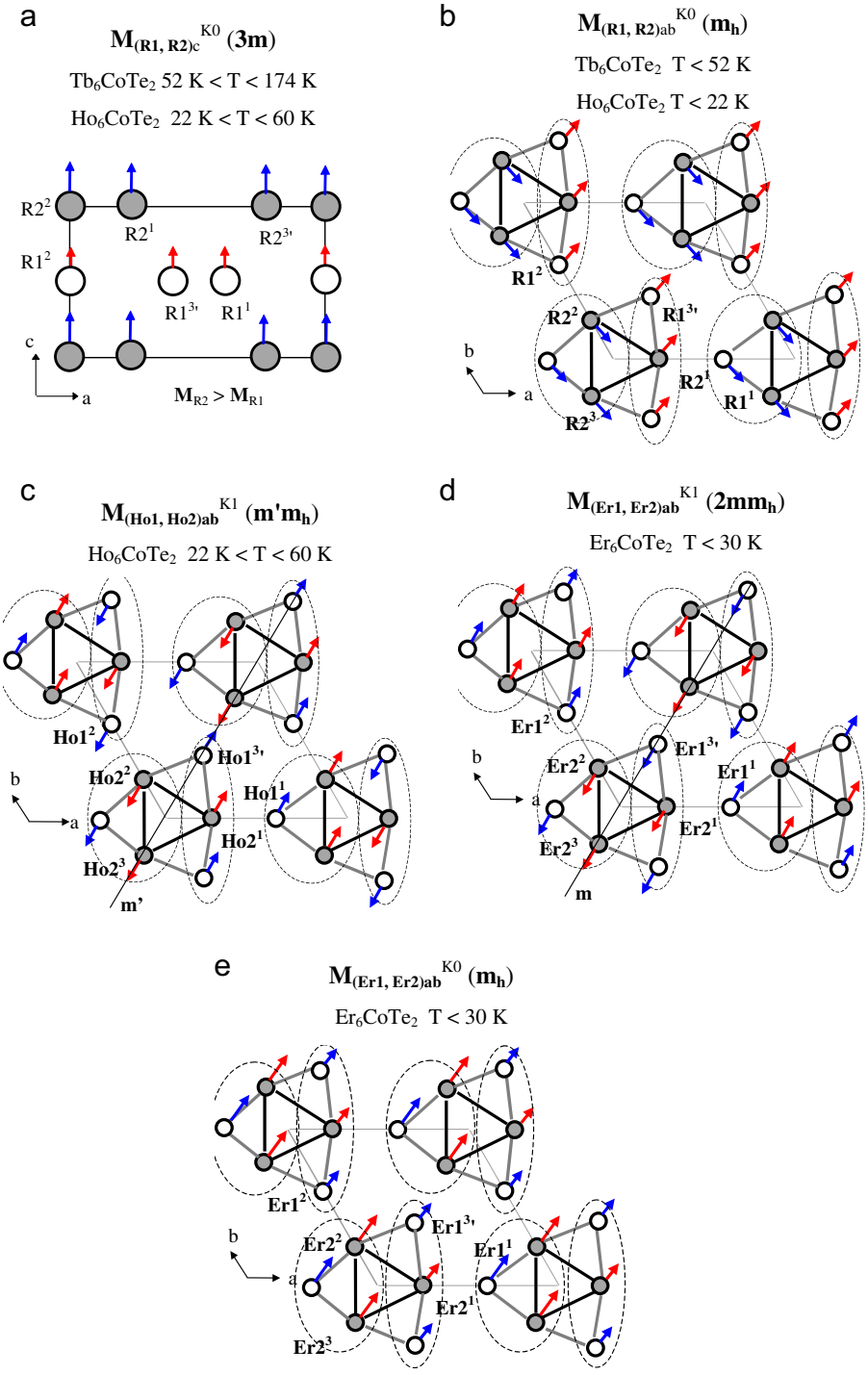

Fig. 10. Magnetic structure of Tb_6CoTe_2 between $T_C=174$ K and $T_{CN}=52$ K (*c*-axis component of Ho_6CoTe_2 below $T_{CN}=60$ K) projected on the *ac* plane ($\mathbf{K}_0=[0, 0, 0]$) (a); projection on the *ab* plane of additional magnetic components of Tb_6CoTe_2 below $T_{CN}=52$ K (*ab* plane component of Ho_6CoTe_2 below $T_N=22$ K) $\mathbf{K}_0=[0, 0, 0]$) (b); high-temperature magnetic *ab* component of Ho_6CoTe_2 between $T_{CN}=60$ K and $T_N=22$ K ($\mathbf{K}_1=[1/2,1/2,0]$) (c); the erbium *ab* plane magnetic component with $\mathbf{K}_1=[1/2,1/2,0]$ (d) and with $\mathbf{K}_0=[0, 0, 0]$ (e) of Er_6CoTe_2 below $T_{CN}=30$ K.

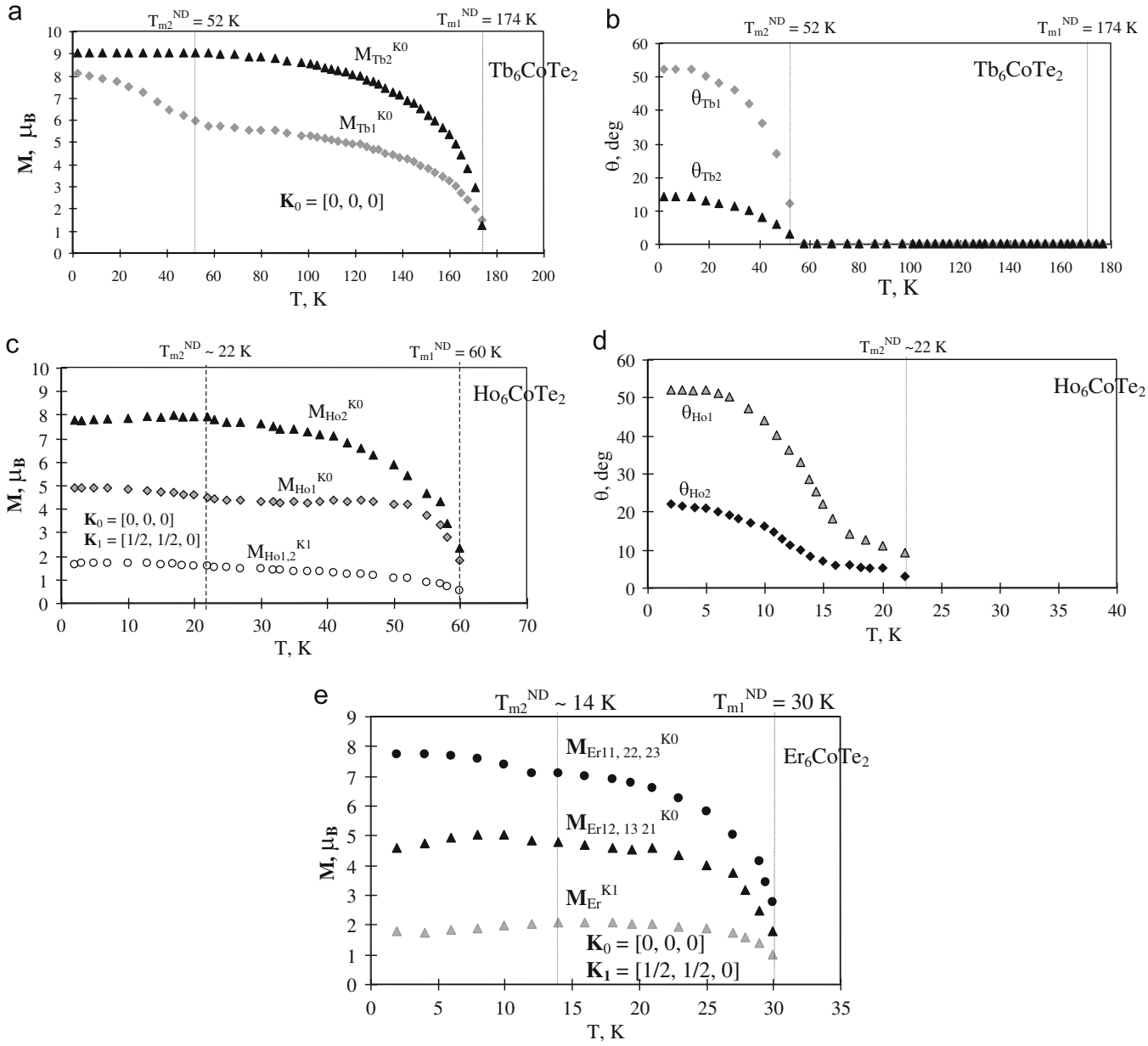

Fig. 11. Thermal variation of the *R*1 and *R*2 magnetic moments and their angles with respect to the *c*-axis in Tb_6CoTe_2 (a, b), Ho_6CoTe_2 (c, d) and Er_6CoTe_2 (e).

magnetic transition at ~ 14 K. Below this temperature the $M_{Er11,22,23}^{K0}$ erbium magnetic component increases, whereas the $M_{Er12,13,21}^{K0}$ and M_{Er}^{K1} magnetic components decrease. Both, the high-temperature and low-temperature magnetic structures of Er_6CoTe_2 belong to the m_h point group. The magnetic structure projected onto the *ab* plane consists of collinear, ferromagnetically ordered domains, like in Tb_6CoTe_2 and Ho_6CoTe_2.

The rare-earth sublattice in R_6CoTe_2 consists of semi-isolated clusters (3*R*1–3*R*2) (Fig. 1b). In general, the magnetic structure of the (3*R*1–3*R*2) cluster includes two *ab*-oriented domains with collinear ordering of the magnetic moments ($M_{R11ab} \uparrow\uparrow M_{R22ab} \uparrow\uparrow M_{R23ab}$ and $M_{R12ab} \uparrow\uparrow M_{R13ab} \uparrow\uparrow M_{R21ab}$) (Figs. 10b–e) and two *c*-oriented domains with magnetic moments of a different magnitude ($M_{R11c}=M_{R12c}=M_{R13c}$ and $M_{R21c}=M_{R22c}=M_{R23c}$) (Fig. 10a). In general, the magnetic structure of R_6CoTe_2 consists of such clusters with magnetic moments of different magnitude and direction from cluster to cluster.

3.4.3. Thermal expansion of crystal lattice of Tb_6CoTe_2

The neutron diffraction data from 290 K down to 2 K for Tb_6CoTe_2 permit us to trace changes in the unit cell parameters with temperature (Fig. 12). The *a*, *c* parameters, *c*/*a* and unit cell volume, *V*, increase with temperature. The high-temperature magnetic ordering at 174 K is accompanied by drops in *a*, *c* and *V*, whereas the low-temperature magnetic ordering at 52 K show no anomalies for these parameters. The Tb_6CoTe_2 phase may be interesting as a potential magnetostrictive material, but the present data must be confirmed by high-resolution diffraction studies.

4. Conclusion

Formation of the Fe_2P-type R_6CoTe_2 compounds from the Mg-type rare-earth metals [6] is shown to modify the magnetic structure of the parent elements. While magnetic orderings in

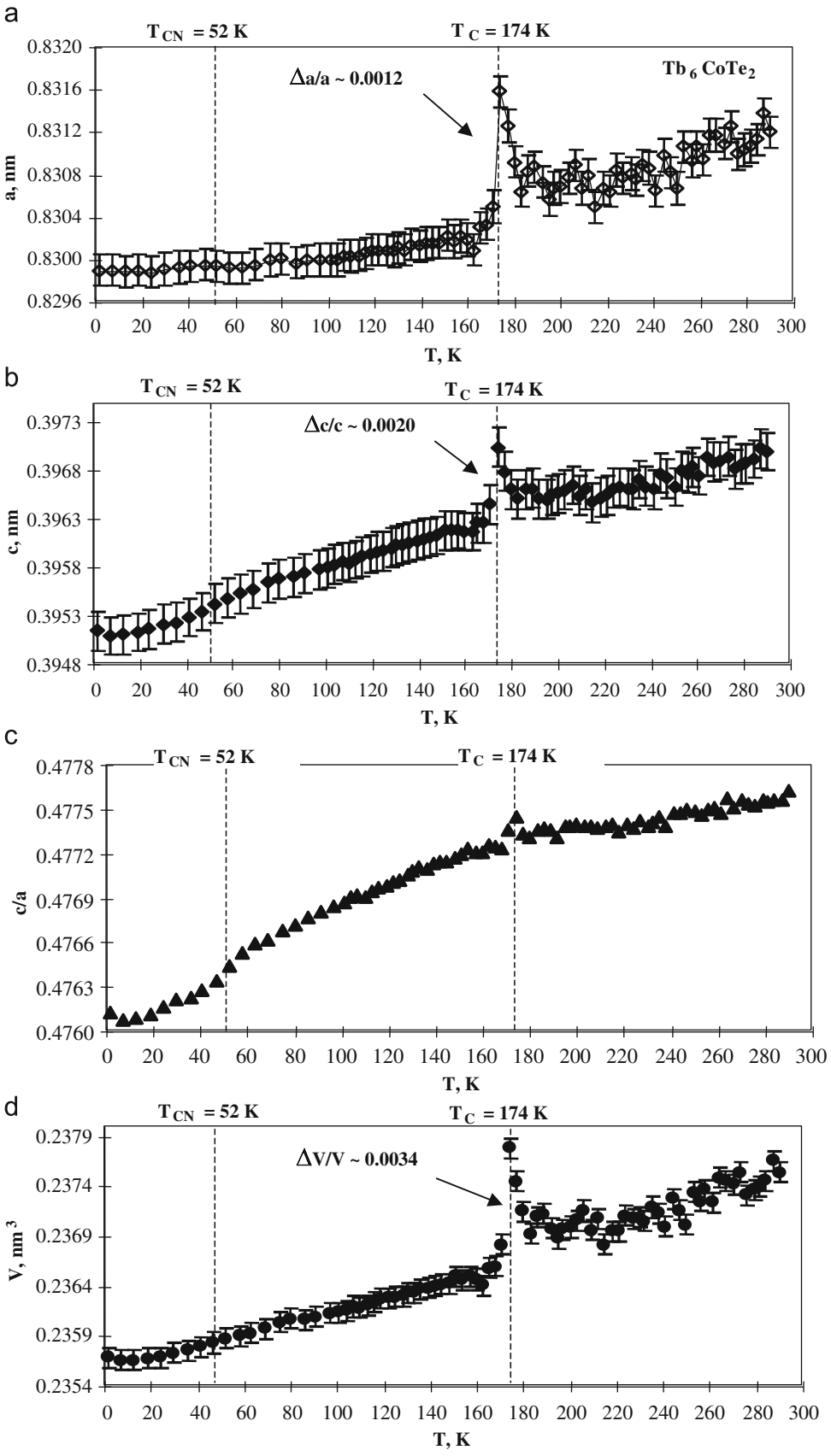

Fig. 12. Thermal variation of the *a* and *c* cell parameters, *c*/*a* ratio and unit cell volume, *V*, for Tb_6CoTe_2.

R_6CoTe_2 are lower in temperature than those of the pure rare-earth metals, the current modification of the Mg-type lattice facilitates ferromagnetic orderings and suppresses antiferromagnetic ones. In general, the high-temperature magnetic transitions correspond to ferromagnetic orderings and low-temperature ones coincide with the reorientation of magnetic moments and increase in the antiferromagnetic component.

The R_6CoTe_2 compounds have a small magnetocaloric effect, but their magnetostriction properties appear to be interesting.

Acknowledgments

This work was supported by the Institut Laue-Langevin in experiments no. 5-31-1908.

This work was supported by the Russian Fund for Basic Research through the project no. 09-03-00173-a. This work was supported by the Indo-Russian Fund for Basic Research through the project no. 09-03-92653-IND_a.

This work supported by a ICDD Grant no. 05-07. The crystallographic data of Ho_6CoTe_2 was used with permission-© JCPDS-International Centre for Diffraction Data.

References

[1] A.V. Morozkin, J. Alloys Compd. 353 (2003) L16–L18.
[2] A.V. Morozkin, J. Alloys Compd. 358 (2003) L9–L10.
[3] A.V. Morozkin, J. Alloys Compd. 360 (2003) L1–L2.
[4] Fanqin Meng, Carmela Maliocchi, Timothy Hughbanks, J. Alloys Compd. 358 (2003) 98–103.
[5] A.V. Morozkin, V.N. Nikiforov, B. Malaman, J. Alloys Compd. 393 (2005) L6–L9.
[6] A.V. Morozkin, R. Nirmala, S.K. Malik, J. Alloys Compd. 394 (2005) 75–79.
[7] A.V. Morozkin, J. Alloys Compd. 395 (2005) 7–16.
[8] Wei He, Jiliang Zhang, Lingmin Zeng, Pingli Qin, Gemei Cai, J. Alloys Compd. 443 (2007) 15–19.
[9] F. Izumi, R.A. Young (Eds.), The Rietveld Method, Oxford University Press, Oxford, 1993 (Chapter 13).
[10] 〈www.ill.eu〉, Yellow Book.
[11] J. Rodriguez-Carvajal, Physica B 192 (1993) 55–69.
[12] J. Emsley, in: The Elements, second ed, Clarendon press, Oxford, 1991.
[13] A.M. Tishin, Y.L. Spichkin, The Magnetocaloric Effect and Its Applications, Institute of Physics Publishing, Bristol, Philadelphia, 2003 480 pp.
[14] V.K. Pecharsky, K.A. Gschneidner Jr., Phys. Rev. Lett. 78 (1997) 4494–4497.
[15] P.S. Kireev, Introduction of theory group and it's application in solid state physic, Moscow, High School, 1979 (in Russian).
[16] S. Legvold, in: E.P. Wohlfarth, (Ed.), Rare Earth Metals and Alloys, Ferromagnetic Materials, vol. 1, North-Holland Publishing Company, Amsterdam, 1980, pp. 183–295.